ELSEVIER

Journal of Power Sources 58 (1996) 7–14

JOURNAL OF POWER SOURCES

Voltage and capacity stability of the Hubble telescope nickel–hydrogen battery

Hari Vaidyanathan [a,*], Harry Wajsgras [b], Gopalakrishna M. Rao [b]

[a] *COMSAT Laboratories, Clarksburg, MD 20871, USA*

[b] *NASA Goddard Space Flight Center, Greenbelt, MD 20771, USA*

Received 14 July 1995; accepted 27 July 1995

Abstract

The power system of the Hubble Space Telescope includes two orbital replacement units, each containing three nickel–hydrogen ($Ni–H_2$) batteries of 88 Ah capacity. Since launch in April 1990, the batteries have completed 23 000 charge and discharge cycles and continue to meet the power demands of the satellite. The voltage, capacity, and pressure characteristics of all six batteries were analyzed to determine the state of health of the battery and to identify any signs of performance degradation. The battery pressures have changed to varying degrees. The end-of-charge pressure for battery 4 increased by 96 psi, while that for battery 3 decreased by 37 psi. The voltages of the individual cells show a decay rate of 0.69 mV per 1000 cycles, and the capacity of the batteries has apparently decreased, possibly due to the system being operated at a lower stage of charge. Autonomous battery operation involving charge termination at a preselected voltage continues to restore the energy dissipated during each orbit. The accumulated data on voltages and recharge ratios can be used to design new temperature-compensated voltage levels for similar missions that employ $Ni–H_2$ batteries.

Keywords: Nickel; Hydrogen; Hubble telescope; Stability; Batteries

1. Introduction

The use of nickel–hydrogen ($Ni–H_2$) batteries in the Hubble Space Telescope (HST) marked another milestone for this electrochemical system, which until the HST launch had been limited to use in geostationary satellites [1–3]. The HST batteries provide an excellent opportunity to discern subtleties in performance that arise when batteries are subjected to frequent on/off cycles. They also yield valuable information on updating battery designs and refining operating details. Based on preliminary assessment of the in-orbit behavior of the $Ni–H_2$ battery, Nawrocki et al. [4] presented their observations on recharge ratios, voltage, and pressure. Subsequently, the batteries have been cycled thousands of times and have endured changes in both temperature and recharge durations, as well as in parameters such as pressure, voltage, and capacity. This paper assesses the performance features of the battery and identifies circumstances and operational modes that are likely to introduce performance anomalies and reduce battery life. It is widely acknowledged that early detection of anomalies, combined with proper battery management, is the key to prolonging battery life.

2. Battery design

The HST power system consists of solar arrays, a power control unit, and two battery orbital replacement units (ORUs). Each ORU contains three $Ni–H_2$ batteries, each with 23 cells of 93 Ah (to 0.1 V) capacity. Only 22 of the cells are serially connected. The cell consists of an electrode stack containing 48 positive plates, with negative plates and Zircar™ separators arranged in a back-to-back configuration. This design is enclosed in a cylindrical pressure vessel with hemispherical ends. The positive plates are of the aqueous, electrochemically impregnated type with dry sintered plaque. The cell contains 27% KOH and a hydrogen precharge. Each cell is encased in an aluminum sleeve to aid in heat dissipation, and is mounted on a baseplate, forming a rectangular structure. Five thermistors and two strain gages on each battery monitor temperature and pressure, respectively. The battery capacity is 93 Ah, and the total weight of the six batteries, divided into two distinct modules, is 427 kg. The end-of-

* Corresponding author.

SSDI 0378-7753(95)02253-D

Table 1
Hubble Space Telescope battery operating parameters

Parameter	Value
Temperature	0±3 °C
Charge rate, (max)	5–18 A
Charge control	V/T level K_1L_4
Total load	1625–2400 W
Reconditioning load	5.1 Ω per 22 cell battery
Discharge model	All batteries in parallel

charge (EOC) and end-of-discharge (EOD) hydrogen pressures expected at 0 °C were 1200 and 200 psi, respectively.

3. In-orbit management scheme

The two-battery modules are connected to the spacecraft power buses, and each battery (22-cell unit) can be switched in or out of the circuit. The battery undergoes 15 cycles over a 24 h period, during which the charge and discharge durations vary from 61 to 70 min and 26 to 35 min, respectively. Charging is accomplished by a temperature-compensated, voltage-limited (V/T) technique in which each battery is charged to a constant voltage corresponding to V/T level K_1L_4 (1.488 V per cell at 0 °C) [2]. The trickle charge duration varies, depending on the shadow period the HST experiences. The battery discharge rate also varies, with a maximum of 20 A. The battery management philosophy is as follows:

1. avoid a temperature rise by minimizing overcharge;
2. cycle the battery between 70 and 88% state-of-charge, and
3. periodically recondition the batteries individually.

The reconditioned battery is not used to support the load in eclipses immediately after the reconditioning discharge, since several sunlight periods are necessary to charge the battery to the preselected voltage. The battery operating parameters are given in Table 1.

4. Voltage behavior

The voltages of all six batteries are continuously monitored to detect any deviations and to accumulate data on the EOC and EOD voltages on each orbit. Fig. 1 shows the variation in the EOD voltage (the calculated average for the cells in six batteries) with cycling. Curve-fitting indicates a decay rate of 6.99×10^{-4} mV per cycle. Examination of Fig. 1 also reveals a greater decline in voltage between 20 000 and 22 500 orbits, which is due largely to changes in the depth-of-discharge, and marginally to an increase in the rate of the degradation processes at the positive plate and to water loss from the electrode stack due to evaporation. The magnitude of voltage reduction is not significant, and the data show a comfortable margin in voltage, with no sign of anomalous degradation. The deviation from the average EOD voltage for the cells in each of the six batteries was examined, and results are presented in Fig. 2. A difference of 8.6 mV was noted among the six voltages, which is not significant.

5. Temperature trends

The batteries are configured to operate isothermally, and their measured temperature is included in calculating the voltage used for charge termination in each orbit. Fig. 3 shows the variation in the calculated average for the maximum temperature shown for the six batteries with cycling. The average value is remarkably stable. The thermal gradient among the batteries is represented as the spread, or ΔT, among the six batteries, and its variation is also shown in Fig. 3. The gradient was 2.6 °C at orbit 7500, and has decreased to the 1–1.5 °C range beyond 20 000 orbits, which is an excellent value. The temperature data indicate that the batteries are unlikely to experience different charge efficiencies, and that the original goal of isothermal condition has been met.

6. Load-sharing and depth-of-discharge

The six batteries support an average load of 2015 W, which is expected to be shared equally. Under normal operation, the load share varied from 16 to 17.5% for each of the six batteries. The change in load-sharing by the batteries with cycling is recorded in Table 2. The data show that load-sharing increases marginally for batteries 1, 2, and 3, and decreases marginally for batteries 4, 5, and 6. Batteries 2 and

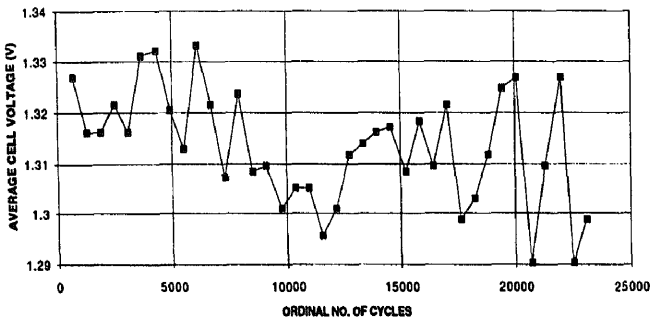

Fig. 1. Variation in EOD voltage with cycling.

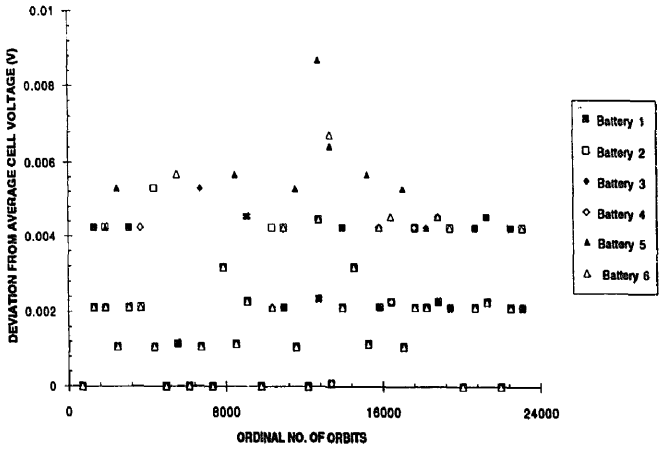

Fig. 2. Deviation in EOD voltage with cycling.

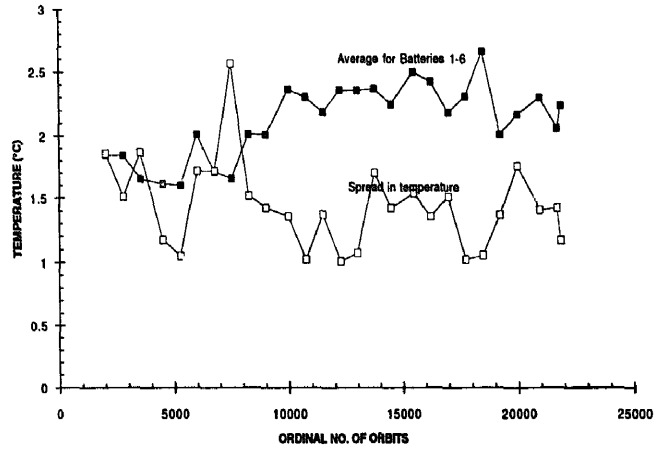

Fig. 3. Variation in temperature of batteries 1 through 6 with cycling.

Table 2
Variation of load-sharing (%)

Battery No.	Orbit 100	Orbit 21050
1	16.5	16.9
2	17.2	17.5
3	16.8	17.0
4	16.7	13.6
5	16.2	16.0
6	16.2	16.0

3 have been sharing a slightly higher fraction, and batteries 5 and 6 a slightly lower fraction, of the load since the beginning of operation. This inequity in sharing is negligible and is attributed to differences in individual cell voltages, diode voltage, and harness loss. However, load-sharing changes significantly when the batteries are reconditioned, since a reconditioned battery is not connected until it has been charged to the K_1L_4 voltage limit, which requires several orbits. For example, the load share increased by about 3% for batteries 1 and 4 in August–September 1992, when the other four batteries were undergoing reconditioning.

The depth-of-discharge of the batteries has been in the range of 5 to 9% since launch. The variability is attributed to the length of the shadow period for the satellite. The depth-of-discharge maximizes to 27% in solar-array feathering tests, and decreases to 5% during hardware-safe mode. Fig. 4 is a historical plot of the depth-of-discharge which assumes a capacity of 88 Ah for each battery. The sinusoidal nature of the curve is due to the change in beta angle, which in turn changes the eclipse duration.

7. Adequacy of voltage-limited charging

The batteries are charged during sunlight periods at constant current to one of eight selectable *V/T* levels, designated

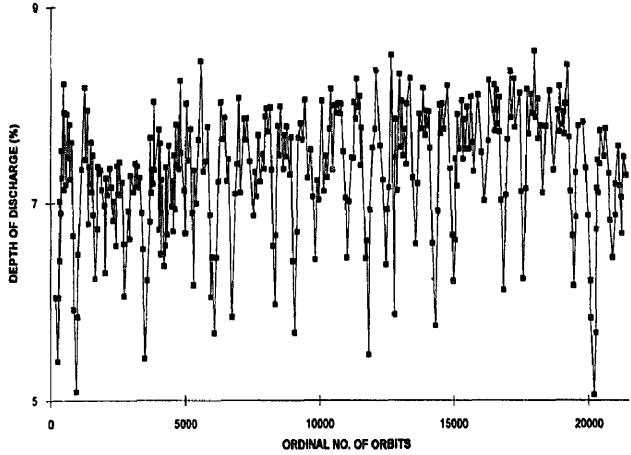

Fig. 4. Variation in depth-of-discharge with cycling.

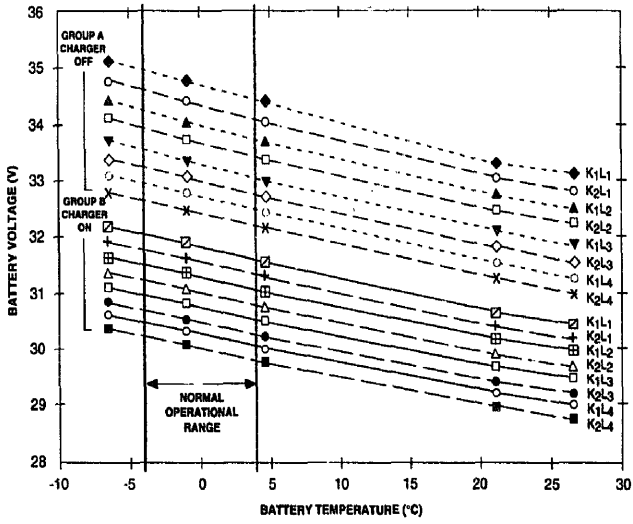

Fig. 5. Charge-current controlers K_1 and K_2 level *V/T* curves.

K_1L_1, K_2L_1, K_1L_2, K_2L_2, K_1L_3, K_2L_3, K_1L_4, and K_2L_4, with the cutoff voltage being highest at K_1L_1 and lowest at K_2L_4. Fig. 5 shows the *V/T* levels, which are plots relating battery voltage to temperature. The plots in group A show the *V/T* levels used to terminate the charge, while those in group B show the voltages below which the charger is activated. Initially, a higher voltage cutoff value (level K_2L_3) was selected to terminate the charge. This was reduced in March 1993 to the present level of K_1L_4. There are two charge-control modes available:

1. Normal hardware-control mode, in which the charge-current controllers (CCCs) sense their associated battery voltage and open a K_1 or K_2 relay when the battery voltage reaches the limit defined by the CCC *V/T* level setting of L_1, L_2, L_3, or L_4. Each K_1 relay open-circuits two-solar panel assemblies (SPAs); each K_2 relay controls one SPA.
2. Computer-controlled charge mode, in which the output of a K_1 or K_2 relay is used to initiate a stored command sequence that removes a sufficient number of SPAs from the buses to reduce the total battery charge current so that each battery will be trickle-charged at ≤ 2 A. This method uses a different set of relays, called solar-array trim relays, to open-circuit the SPAs.

The computer-controlled charging scheme was used between launch (April 1990) and March 1993. Due to the failure of two of the solar-array trim relays required to implement the computer method, the hardware-charge method has been used since that time.

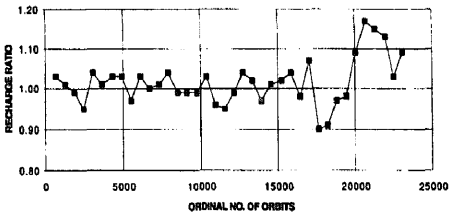

Fig. 6. Variation in recharge ratio for battery 1.

The charge input in each orbit is calculated based on the switching time of the relay. The plot in Fig. 6, which depicts the variation of recharge ratio, was constructed by factoring the discharged capacity. The recharge ratio has varied from 0.96 to 1.04, with a median value of 1.02. Thus, the voltage-limited charging technique has worked well during eclipse cycling. However, the recharge following reconditioning is requiring several orbits to complete due to the limit on current and voltage. When unbalanced load-sharing occurs as a result of reconditioning, the option of charging the batteries at a higher V/T level soon after reconditioning to reduce charging time should be considered.

8. In-orbit reconditioning and capacity determination

The battery design includes a provision for discharging the battery through 5.1 Ω to determine capacity, and for reconditioning. The beneficial effects of reconditioning in-orbit batteries by draining through a resistor and recharging has been demonstrated [5,6]. The major advantages of periodic reconditioning include equalization of the state-of-charge in the cells, reduction in pressure, improved electrolyte distribution in the electrode stack components, and occasionally an improvement in the average discharge voltage. All the batteries have completed two reconditioning discharges, except for battery 4 which has completed only one. In 1990, discharge was to 18 V; in 1994 the limit was lowered to 15 V.

Figs. 7 and 8 compare the voltage and pressure profiles obtained for battery 1 during the capacity determination in 1994 versus those obtained in 1990. The data show a 16 Ah decrease in capacity to 26.4 V. The beginning of discharge capacity, as calculated from the EOC pressure, was 96 Ah in 1994 and 94 Ah in 1990, and capacity obtained by resistive discharge was 80 Ah in 1994 and 96 Ah in 1990. A similar degradation in capacity was observed for other batteries in the second reconditioning.

Table 3 summarizes the reconditioning data, which include the capacity calculated using reconditioning current, as well as pressure and the duration of sunlight prior to reconditioning. The calculation of capacity from pressure assumed a factor of 10.33 psi/Ah, which was derived from the test data obtained prior to launch. The capacity calculated using current is considered more accurate. An increase in the duration of sunlight translates into an increase in the trickle charge

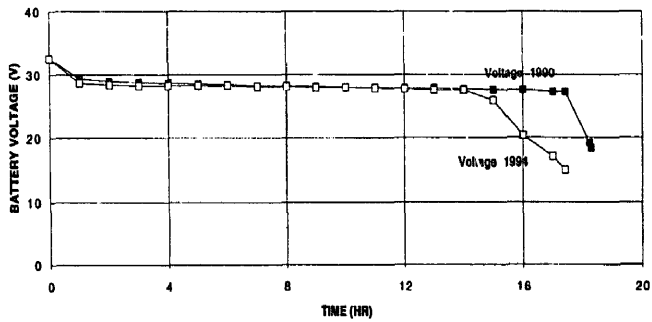

Fig. 7. Voltage profiles for battery 1 during reconditioning.

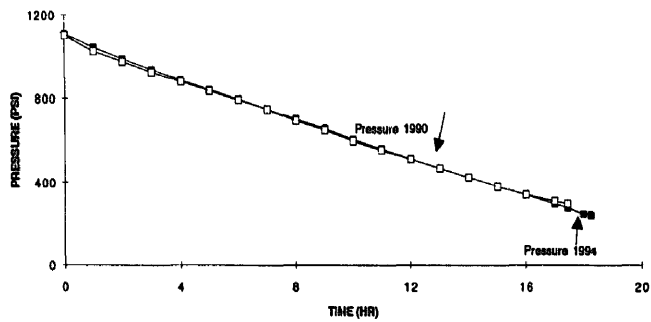

Fig. 8. Pressure profiles for battery 1 during reconditioning.

Table 3
Reconditioning parameters for Hubble Space Telescope Ni–H_2 batteries

Battery No.	Reconditioning date	Cycles	Voltage limit V/T level	Sunlight time (min)	Capacity calculated from current to 26.4 V (Ah)	Capacity calculated from pressure to 26.4 V (Ah)	End of reconditioning voltage (V)
1	12/90	3383	1.504	69.0	94.2	93.0	19
	8/94	21900	1.488	62.0	80.4	94.4	15
2	8/92	12940	1.504	61.3	88.5	94.0	13
	12/94	23700	1.488	69.8	79.3	82.2	15
3	8/92	12940	1.504	61.3	85.6	92.3	13
	4/95	25500	1.488	61.4	73.5	82.2	15
4	12/90	3383	1.504	69.0	88.0	93.4	19
5	8/92	12940	1.504	61.6	94.0	102.6	13
	2/95	24600	1.488	61.2	78.3	94.8	15
6	8/92	12940	1.504	61.2	88.3	93.9	13
	10/94	22890	1.488	65.5	74.6	86.5	15

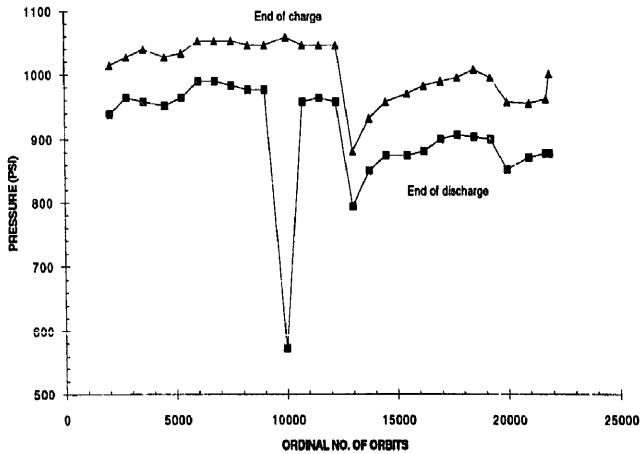

Fig. 9. Variation of pressure with cycling for battery 3.

duration which potentially increases the charge input. There is evidence that battery 2 recovered some lost capacity due to an increase in sunlight time, as recorded in Table 3.

9. Pressure changes

The hydrogen pressure in one cell in each battery is continuously monitored to obtain information on the state-of-charge of the battery, as well as to track the capacity remaining at the EOD in each orbit. The typical value for pressure at EOC during ground testing was 1100 psi. The EOD to 1 V pressure was 200 psi. Cell pressure decreases when the battery is subjected to deep-discharge reconditioning, but never reaches zero because of the hydrogen precharge. The pressure at the end of voltage-limited charging following reconditioning is low, and increases with each recharge. The decrease in EOC and EOD pressures at orbit 12 758 is due to reconditioning. The pressure rise, and the resultant increase in state-of-charge followed by stabilization, which occurs after reconditioning, is evident in Fig. 9. The battery pressure at EOC is plotted in Fig. 9 for battery 3 as a function of the number of orbits.

The dependence of pressure on repeated charge and discharge is different for the six batteries. The EOC pressure increased by 9.5 to 29.5 psi for batteries 1, 4, 5, and 6, whereas the pressures of batteries 2 and 3 decreased by 13 to 38 psi with cycling. Similarly, the EOD pressure increased by 20 to 98 psi for batteries 1, 4, 5, and 6, and decreased by 37 to 60 psi for batteries 2 and 3. If the pressure data for the batteries are compared with data obtained in ground tests, it becomes evident that only battery 1 has reached or exceeded the initial pressure obtained for the EOC. Battery 1 yielded 1118 psi at cycle 22 000, which is only 18 psi higher than the ground test value. A significant increase was observed in the EOD pressure for battery 4 due to a general increase in the state-of-

Table 4
Results of destructive physical analysis

Item	Result	Comments
Cell capacity	89 Ah to 1 V (96.9 Ah to 0.1 V) at 0 °C	Negligible degradation
Self-discharge	Retained 88% of capacity	Represents no degradation
Discharge voltage	Discharge voltage is lower by 10–40 mV for at least 50% of the discharge duration	Indicates corrosion of sintered nickel and water loss from stack
Positive plate	Active material utilization of 106% in flooded KOH and 103.7% in the cell. Minor extrusions of active material	Good values
Electrolyte	Positive plates contained more electrolyte than in cells of similar design. Carbonate content 2.3 wt.%	Behavior compares favorably with that for cycled cells
Separator	Good condition, with an absorbency of 2.2 g KOH/g and resistivity of 2.6 Ω cm	Good values
Negative plate	Anode polarization was 60 mV at 50 mA/cm^2	No degradation

charge of the battery at EOD, corrosion of the sinter structure in the positive plate, and drift in the strain gage readings. Of these, the most potentially life-limiting is corrosion.

There are several reasons for the capacity decrease exhibited by the batteries. Initially, it appears to be due to the lower state-of-charge of the batteries prior to the reconditioning discharge. However, one cannot preclude corrosion of sintered nickel, which produces oxidized nickel species that not only compete for KOH and H_2O, but also block electrolyte access to the active material. In addition, structural changes occur in the positive plate, such as movement of active material from the center of the plate to the edges, with eventual extrusion. It is important to monitor the pressure, average discharge voltage, and battery capacity to determine whether the rate of corrosion or other degradation has accelerated, and to determine whether the capacity decline is permanent or reversible. The periodic resistive discharges planned for the batteries are a step in that direction.

10. Destructive physical analysis

A representative cell was cycled in a regime that mimics in-orbit conditions, and then was destructively analyzed at the end of 5.5 years of testing in ground test facilities. The cell yielded 89 Ah and retained 88% of capacity when subjected to self-discharge at 10 °C. Both values are very good. The electrode stack was dimensionally unchanged and clean outside. Disassembly of the stack components indicted burn marks on some negative plates, which could be attributed to the excessive heat generated when hydrogen reacts very rapidly with oxygen during overcharge. There was also evidence of extrusion of active material from the positive plates, and greater than expected swelling. The swelling of the plates could not be quantified, since an uncycled cell was not subjected to such an analysis. However, high-rate cycling of representative plates showed the swelling to be 10%, which indicates that the positive plates are susceptible to more than the expected 3% swelling. Destructive physical analysis of an uncycled representative cell is planned. The electrolyte distribution in the components was uniform, and the carbonate content was 2.3%. The positive active material loading level was 1.51 g/cm^3, and its coefficient of utilization was 106% in flooded KOH and 103.7% in the cell, which compares favorably with data for plates from sparingly cycled cells. The absorbency of the separator was 2.2 g KOH/g of separator, which is a good value. Table 4 summarizes the results of the destructive physical analysis. The cell shows the expected component wear, and its performance does not raise any concerns about life expectancy.

11. Discussion

The Hubble Space Telescope is specified to be a 15-year satellite, and periodic replacement of its batteries is anticipated. The battery behavior discussed here points to a high level of voltage performance, with stable recharge ratios and temperature. The voltage decay trend indicates that the battery will continue to cycle in this fashion for several more years, barring catastrophic failures such as leakage or electrical short. There is some nonuniformity in the pressure behavior, and a pressure increase at the EOD has been observed. The capacity measured during reconditioning has decreased for all the batteries; however, this only marginally increases the depth-of-discharge during each eclipse and, in view of the built-in overcapacity, is not of serious concern for the mission. Furthermore, the decrease in capacity observed can be confirmed as a permanent loss only if the battery capacity decreases again in the next reconditioning discharge.

The battery behavior does not warrant any changes in the in-orbit management parameters, such as the *V/T* level for charge control, depth-of-discharge, and reconditioning parameters. Ground tests are in progress to determine whether operating the battery at a lower temperature (−4 to −2 °C) to increase the EOC voltage would recover some of the lost capacity. Destructive physical analysis of the cell subjected to cycling in the laboratory supports the contention that the decreases in capacity and EOD voltage are traceable to degradation mechanisms occurring at the positive plate — most importantly, extrusion of the active material. The voltage

decay attributable to water loss from the electrode stack is reversible, and the periodic reconditioning which decreases the hydrogen pressure to very low values, in combination with the low operating temperatures, is expected to drive water back to the stack.

Acknowledgements

Financial support for this work was provided by the NASA Goddard Space Flight Center. The authors are grateful to M. Williamson of Computer Sciences Corporation for assembling the in-orbit performance data.

References

[1] D.E. Nawrocki et al., *Proc. 25th Intersociety Energy Conversion Engineering Conf. (IECEC), Reno, NV, USA, 1990*, Vol. 3, American Chemical Society, Washington, DC, p. 1.

[2] J. Dunlop, G. Rao and T. Yi, *NASA Handbook for Nickel–Hydrogen Batteries, NASA Ref. Pub. No. 1314*, 1993, pp. 2–4.

[3] H. Vaidyanathan and J. Dunlop, *Proc. 21st Intersociety Energy Conversion Engineering Conf. (IECEC), San Diego, CA, USA, 1986*, American Chemical Society, Washington, DC, p. 1560.

[4] D. Nawrocki et al., *Proc. NASA Aerospace Battery Workshop, NASA Conf. Pub. No. 3192*, 1992, pp. 507.

[5] J. Dunlop, A. Dunnet and D. Cooper, *Proc. 27th Intersociety Energy Conversion Engineering Conf. (IECEC), San Diego, CA, USA, 1992*, Vol. 1, p. 117.

[6] M. Earl, T. Burke and A. Dunnet, *Proc. 27th Intersociety Energy Conversion Engineering Conf. (IECEC), San Diego, CA, USA, 1992*, Vol. 1, p. 127.